The 15th International Symposium on Magnetic Bearings, August 3-6, 2016, Mojiko Hotel, Kitakyushu, Japan

ISMB15

Identification of Parameters in Active Magnetic Bearing Systems

Andreas JAUERNIK VOIGT[*,**], Jonas LAURIDSEN[**], Christian MANDRUP-POULSEN[**], Kenny KROGH NIELSEN[*] and Ilmar F. SANTOS[***]

[*] Lloyd's Register Consulting
Copenhagen, Denmark

[**] Dept. of Mechanical Eng., Technical University of Denmark
Copenhagen, Denmark

[***] Dept. of Mechanical Eng., Technical University of Denmark
Copenhagen, Denmark

E-mail: ifs@mek.dtu.dk

Abstract

A method for identifying uncertain parameters in Active Magnetic Bearing (AMB) based rotordynamic systems is introduced and adapted for experimental application. The Closed Loop Identification (CLI) method is utilised to estimate the current/force factors $\mathbf{K}_i$ and the displacement/force factors $\mathbf{K}_s$ as well as a time constant τ_e for a first order approximation of unknown actuator dynamics. To assess the precision with which CLI method can be employed to estimate AMB parameters the factors $\mathbf{K}_i$, estimated using the CLI method, is compared to $\mathbf{K}_i$ factors attained through a Static Loading (SL) method. The CLI method and SL method produce similar results, indicating that the CLI method is able to perform closed loop identification of uncertain AMB parameters.

Keywords: Rotordynamics, Parameter identification, Closed-loop, Experimental, Active Magnetic Bearings.

1. Introduction

Active Magnetic Bearings (AMBs) are commonly employed in turbomachinery applications, due to their many advantages over conventional bearing elements (Schweitzer, 2002). The operability of AMB based rotordynamic systems are dependent on a well performing feedback control scheme. This highlights the need for a precise mathematical model of the AMB-rotor system as this lays the foundation for both controller design and performance evaluation of the overall rotordynamic system. Uncertainties in AMB parameters and unmodelled AMB dynamics are sources of inconsistencies between the physical AMB system and its mathematical representation. The uncertain parameters are commonly electromechanical in nature and the uncertainties originate from production tolerances, misalignment issues and variations in material specifications, among others. Conventionally unmodelled AMB dynamics include the formation of Eddy currents which can influence the electrodynamic behaviour of the AMB actuators. To achieve the necessary level of model certainty for ensuring satisfactory performance of the AMB system, it is often necessary to identify the uncertain parameters and relevant dynamical effects experimentally, preferably in-situ, and update the mathematical model accordingly. However, as AMB based rotordynamic systems are inherently open loop unstable and requires feedback control to operate, measurement noise embedded in the system outputs, e.g. in the rotor displacement signals, can not be assumed uncorrelated with system inputs. This entails that applying conventional open loop identification techniques is not suitable (Anderson, 1998). Closed loop identification methods have previously been employed with success (Sun et al., 2014, Sun et al., 2014, Tiwari and Chougale, 2014) and are commonly based on frequency domain techniques to capture rotordynamic system performance. This paper describes a newly developed fast and transparent time domain closed loop identification (CLI) method (Lauridsen et al., 2015) and its application to an industrial scale AMB based rotordynamic testing facility. The testing facility is designed to be used for identifying rotordynamic properties of turbomachinery seals subjected to multiphase flow conditions (Voigt et al., 2016). The CLI method is capable of identifying specific AMB parameters, thus enabling utilization of a-priori knowledge of the AMB-rotor model structure. To illustrate the applicability of the CLI method to AMB-rotor systems the focus of this paper is oriented at identifying AMB force/current factors $\mathbf{K}_i$ and force/displacement factors $\mathbf{K}_s$ experimentally. Additionally, a time constant τ_e for a first order transfer function describing the conventionally unmodelled correlation between imposed coil current and actuator flux formation is identified experimentally. Furthermore, as the CLI method has not previously been applied experimentally to AMB systems, a

subset of the CLI method results are compared to results obtained using a static load (SL) method, in order to assess the capabilities of the CLI method. Specifically, $\mathbf{K}_i$ parameters identified using both methods are reported for comparison.

2. Experimental Facilities

The experimental facilities employed in the underlying work of this paper consists of a AMB-based rotordynamic test bench and a calibration facility presented in Fig. 1(a). The AMBs radially support a symmetric rigid rotor which is driven by an asynchronous motor through an intermediate shaft and a flexible coupling. Angular contact ball bearings, supporting the intermediate shaft housed in the intermediate shaft pedestal, compensate for axial forces acting on the rotor. The radial AMBs are of the eight pole heteropolar type featuring an embedded Hall sensor system which can be utilised to quantify forces exerted on the rotor by the AMBs, see Fig. 1(b). In Fig. 1(b) both the global reference frame denoted by x, y and the actuator reference frame denoted by ζ, η is introduced. The actuators are tilted 45° with respects to the global reference frame. Throughout the paper subscripts ζ, η are used to denote quantities belonging to the actuators aligned with the respective axes of the stator reference frame. The two AMB stators have been manufactured using two different production methods yielding different geometric tolerances for the AMBs. The AMBs are supplied by four commercially available 3 kW switch-mode laboratory amplifiers, not specifically designed for AMB use. The AMBs are controlled using a standard decentralized PID scheme. The calibration facility depicted in Fig. 1(c), includes four controllable pneumatic pistons that can be applied to exert static forces of varying direction and magnitude onto the rotor. Forces are transferred from the pistons to the rotor via a force transducer mounted on the calibration clamp which in turn is mounted on the rotor as seen exemplified for a single piston set-up in Fig. 1(d). A full description of the test facility can be found in (Voigt et al., 2016), which also presents the calibration of the Hall sensor system. Design parameters for the rotordynamic test bench can be found in Table 1.

3. Mathematical Representation of the AMB-Rotor System

The global AMB-rotor system is described mathematically by a rotor model and a model of the two radial AMBs. The rotor is considered rigid in the operating range of the test facility and it is assumed in the modelling that the only significant external forces acting on the rotor originates from the radial AMBs.

3.1. Model of AMB Forces

The forces generated by an AMB acting on the rotor can be described as function of the lateral AMB rotor displacements $\mathbf{s}$ and the imposed control currents $\mathbf{i}_c$. The linearised AMB forces can be represented as (Bleuler et al., 2009)

$$\mathbf{f}_b(\mathbf{i}_c, \mathbf{s}) = \mathbf{K}_i \mathbf{i}_c + \mathbf{K}_s \mathbf{s} \tag{1}$$

in which $\mathbf{K}_i$ are $\mathbf{K}_s$ are matrices containing parameters defined as

$$\mathbf{K}_i = \begin{bmatrix} K_{i,A_\zeta} & 0 & 0 & 0 \\ 0 & K_{i,A_\eta} & 0 & 0 \\ 0 & 0 & K_{i,B_\zeta} & 0 \\ 0 & 0 & 0 & K_{i,B_\eta} \end{bmatrix}, \quad \mathbf{K}_s = \begin{bmatrix} K_{s,A_\zeta} & 0 & 0 & 0 \\ 0 & K_{s,A_\eta} & 0 & 0 \\ 0 & 0 & K_{s,B_\zeta} & 0 \\ 0 & 0 & 0 & K_{s,B_\eta} \end{bmatrix} \tag{2}$$

which defines a dedicated force/current and force/displacement factor for each actuator of the two AMBs. The subscripts A_ζ, A_η, B_ζ, and B_η designates to which AMB and which actuator the factor belongs, respectively, see Fig. 1(b).

Table 1: Design parameters for the rotordynamic test bench

Rotor length	860	mm
Rotor assembly mass	69	kg
1st rotor bending mode @	550	Hz
Stator inner diameter	151	mm
Nominal radial air gap	0.5	mm
Winding configuration	N-S-S-N-N-S-S-N	[-]
Lamination thickness	0.35	mm
Laminate material	SURA M270-35A	
Max. static load capacity (per AMB)	7500	N
Bias current range	4 to 10	A
Number of Hall sensors per AMB	8	
Hall sensor type	F.W. Bell - FH-301	

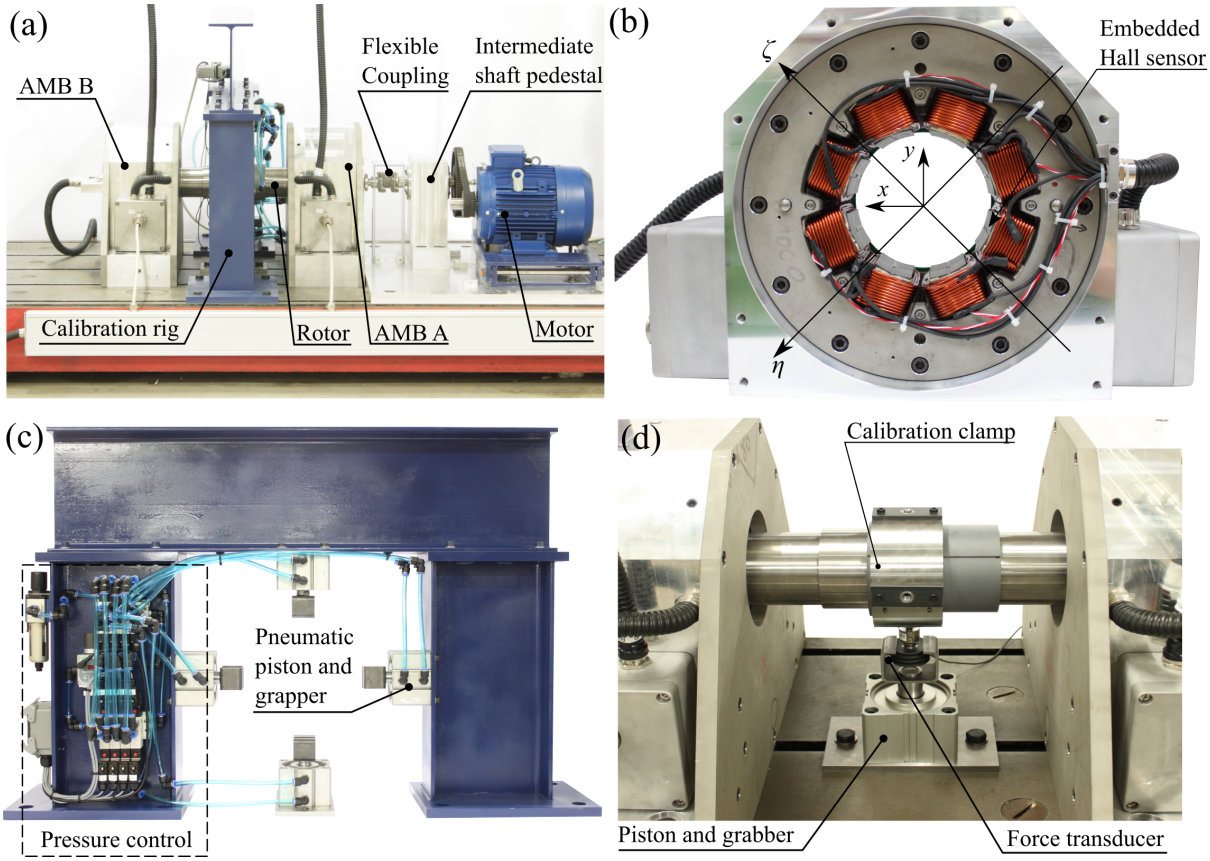

Fig. 1: Experimental facilities used throughout the study. (a) Rotordynamic test bench, showing main components. (b) Test bench AMB showing the placement of the embedded Hall sensors as well as AMB actuator and global reference frame definitions. (c) Calibration facility showing the pneumatic pistons and pressure control unit. (d) Interface between calibration facility and rotor showing a single piston with grabber as well as the calibration clamp mounted on the rotor.

3.2. Rotor Model

The rotor is modelled using a conventional Finite Element (FE) method since the CLI method utilizes the structure of the FE based rotor model for uncertainty representation (Lauridsen et al., 2015). Furthermore, using the FE approach retains generality of the methodology, and by applying modal truncation techniques, real left and right transformation matrices can be determined which allows transforming the full order FE model to reduced form. Here the global rotor model has been truncated to only include rigid modes. It is noted that the shaft is non-rotating through the entirety of the study. The resulting rotor model can be written in state space form as

$$\dot{\mathbf{x}}_f = \mathbf{A}_f \mathbf{x}_f + \mathbf{B}_f \mathbf{u}, \quad \mathbf{y} = \mathbf{C}_f \mathbf{x}_f \tag{3}$$

4. Closed Loop Model and Identification Scheme

The CLI method is based on theory presented in (Lauridsen et al., 2015) and is in this paper adapted for experimental application. The schematic block diagram shown in Fig. 2 acts as the basis for the CLI method, and shows the elements of the global closed loop system in a vectorised formulation where **K** represents the known controller. The electrodynamic model of the AMB actuator contains two first order transfer functions as indicated on Fig. 2. The block denoted "Amplifier and coil" represents a known first order transfer function from the current reference signals to the actual current flowing in the coils, consequently approximating the dynamics originating from the coil inductance and the power amplifier. Similarly, the block "Unknown actuator dynamics" is an assumed first order transfer function with unknown time constant τ_e, which aims at describing the dynamics originating from eddy current formation and unknown amplifier dynamics. The

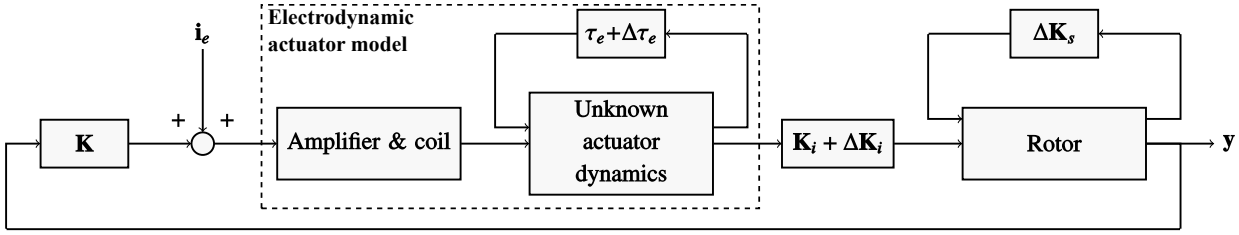

Fig. 2: Closed loop schematic of the AMB-rotor system.

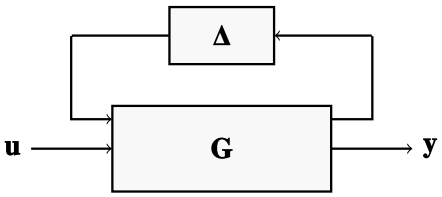

Fig. 3: Uncertain plant representation using upper LFT, $\mathbf{G}_{unc} = \mathcal{F}_u(\mathbf{G}, \mathbf{\Delta})$

unknown time constant appended to the block "Unknown actuator dynamics" is represented by a nominal value τ_e, serving as an initial guess, plus the variation $\Delta\tau_e$. All four actuators share one common time constant τ_e. The current/force factor is here composed of a nominal initial guess $\mathbf{K}_i$ and an appended uncertainty $\Delta\mathbf{K}_i$. The block "Rotor" contains the rotor model with the nominal displacement/force factor $\mathbf{K}_s$ and an actuator uncertainty mapping. The uncertainty mapping describes how a change $\Delta\mathbf{K}_s$ in the nominal displacement/force factor modifies the overall dynamic behaviour of the rotor. The rotordynamic model is represented on reduced modal form and the uncertain parameters of the rotor model, here $\mathbf{K}_s$, is extracted and described using a Linear Fractional Transformation (LFT) which is treated subsequently.

4.1. LFT Representation of Uncertain Rotordynamic Systems

The rotordynamic system with unknown $\Delta\mathbf{K}_s$ is formulated using a LFT as described in this section. To retain generality, the block termed "Rotor" and the block containing $\Delta\mathbf{K}_s$ in Fig. 2 are in the following denoted by $\mathbf{G}$ and $\mathbf{\Delta}$, respectively. The uncertain rotor model $\mathbf{G}_{unc}$ is constructed using the nominal model and the uncertainty representation, which combined is written on LFT form as illustrated in Fig. 3 for the global AMB-rotor model. In Fig. 3 $\mathbf{\Delta}$ denotes a 4×4 diagonal matrix representing $\Delta\mathbf{K}_s$. The matrix $\mathbf{G}$ is constructed as outlined in the following and is described in detail in (Lauridsen et al., 2015). It can be proved that changing a component in $\mathbf{K}_s$, i.e. changing the displacement/force factor for a single actuator direction, imposes a change in a single column with index j of the full order system matrix $\mathbf{A}_f$. The column corresponds to a specific node with index j in the FE representation of the rotor where the AMB forces are imposed on the rotor model. This can be expressed as

$$\mathbf{A}_{\Delta_f} = \begin{bmatrix} 0 & \dots & 0 & a_{1,j} & 0 & \dots & 0 \\ 0 & \dots & 0 & a_{2,j} & 0 & \dots & 0 \\ \vdots & \ddots & \vdots & \vdots & \vdots & \ddots & \vdots \\ 0 & \dots & 0 & a_{i,j} & 0 & \dots & 0 \end{bmatrix} \tag{4}$$

It is assumed that the matrix $\mathbf{A}_\Delta$ expressing the change in the system matrix can be reduced by applying the same modal truncation matrices used to reduce the full order nominal system. This is presented in Eq. (5) and has shown to hold in practice. The matrix $\mathbf{A}_{f,\Delta}$ found in Eq. (4) can be written as the product of the column vector $\mathbf{B}_{f,\Delta}$, the scalar Δ and the row vector $\mathbf{C}_{f,\Delta}$ as shown in Eq. (6). Consequently the input mapping $\mathbf{B}_\Delta$ and output mapping $\mathbf{C}_\Delta$ of the uncertainties in the reduced system is described by Eq. (7).

$$\mathbf{A}_\Delta = \mathbf{T}_L\, \mathbf{A}_{f,\Delta}\, \mathbf{T}_R \tag{5}$$

$$= \mathbf{T}_L \mathbf{B}_{f,\Delta}\, \Delta\, \mathbf{C}_{f,\Delta_f} \mathbf{T}_R \tag{6}$$

$$= \mathbf{B}_\Delta\, \Delta\, \mathbf{C}_\Delta \tag{7}$$

The process outlined above is repeated for each uncertain entry in the current/force matrix $\mathbf{K}_s$. Assembling the columns of $\mathbf{B}_\Delta$ and rows of $\mathbf{C}_\Delta$ and casting $\mathbf{\Delta}$ as an 4×4 diagonal matrix, the complete uncertainty representation illustrated in

Fig. 3 can be determined by (7). The matrix $\mathbf{G}$ can be written on state space form, as shown in Eq. (8), where $\mathbf{A}$, $\mathbf{B}$ and $\mathbf{C}$ are the nominal system matrices on reduced form. Here the input and output matrices are extended from the nominal model to include B_Δ and $\mathbf{C}_\Delta$. Note that no extra system dynamics is added since the LFT only changes the nominal system matrix $\mathbf{A}$.

$$\mathbf{G} = \left[\begin{array}{c|cc} \mathbf{A} & \mathbf{B}_\Delta & \mathbf{B} \\ \hline \mathbf{C}_\Delta & 0 & 0 \\ \mathbf{C} & 0 & 0 \end{array}\right] \tag{8}$$

4.2. Estimation of Optimal Parameters

As indicated in Fig. 2, a Pseudo-Random Binary Sequence (PRBS) current signal $\mathbf{i}_e$ can be imposed to perturb the system model and time domain simulation can be employed to yield the displacement response $\mathbf{y}$, which can be compared to a response quantified experimentally. To estimate the uncertain AMB parameters the CLI scheme is formulated as a minimization problem that iterates through the uncertain parameters to decrease the discrepancy between the simulated response and the experimentally acquired response. The goal is to find the parameters which provides the best fit between simulation data and experimental data. This can be done by finding the global minimum of the cost function shown in Eq. (9) which is defined as the sum of squares of the discrepancy between simulation data and experimental data as

$$J(\boldsymbol{\theta}) = \left\| \mathbf{y}_{meas} - \mathbf{y}) \right\|_2^2 \tag{9}$$

in which $\mathbf{y}_{meas}$ and $\mathbf{y}$ denotes matrices containing the measured and simulated rotor displacements, respectively. The simulated displacements $\mathbf{y}$ can be expressed as

$$\mathbf{y} = \mathbf{T}(\boldsymbol{\theta}) i_e, \text{ where } \boldsymbol{\theta} = \left\{ K_{i,A_\zeta}, K_{i,A_\eta}, K_{i,B_\zeta}, K_{i,B_\eta}, K_{s,A_\zeta}, K_{s,A_\eta}, K_{s,B_\zeta}, K_{s,B_\eta}, \tau_e \right\} \tag{10}$$

where $\mathbf{T}(\boldsymbol{\theta})$ is a transfer function for the closed loop response from the excitation current input $\mathbf{i}_e$ to the displacement $\mathbf{y}$ for a given $\boldsymbol{\theta}$ vector. Minimization of the cost function seen in Eq. (9) has been implemented using MATLAB's `lsqnonlin` function. The CLI method has shown to converge fast towards optimal parameters, even for the specific case where nine parameters are simultaneously identified.

5. Experimental Methodology and Data Post Processing

Two different experimental procedures (CLI and SL) are employed in the study, and both are conduced for the same operation conditions and the same choices of bias currents namely 6 A, 8 A, and 10 A. The experiments are condicted five times for both methods to assess the repeatability of the results. Generating data for the CLI method is relatively straight forward and shortly outlined in the following. The rotor is levitated to the nominal position, and a PRBS disturbance signal is imposed on the control currents, resulting in purely lateral displacement of the rotor, while simultaneously capturing control currents and rotor position signals. The captured signals are used as input for the CLI method to experimentally determine the $\mathbf{K}_i$, $\mathbf{K}_s$ and τ_e parameters.

The secondary experimental SL procedure is introduced with the ultimate goal of obtaining the $\mathbf{K}_i$ parameters, consequently allowing for a comparison with results obtained using the CLI scheme. The basic principle of the alternative experimental procedure is to apply a known load to the centre of the shaft, see Fig. 1(d), using the pneumatic pistons of the calibration facility, see Fig. 1(c), and measure the force and amplifier current signals of all amplifiers. In this case no perturbation of the rotor is imposed, and the force applied to the rotor is quantified using calibrated strain-gauge based HBM U9C force transducers mounted between the pistons and the rotor (Voigt et al., 2016). The applied force is varied in both direction and magnitude, using the four pistons and the pressure control unit seen in Fig. 1(c). Summing forces and moments acting on the rotor allows a set of four equilibrium equations to be established. Furthermore, using Eq. (1) and realizing that the rotor is in static equilibrium, and consequently the variations in rotor displacement is zero leading to $\mathbf{f}_b(\mathbf{i}_c, \mathbf{s}) = \mathbf{K}_i \mathbf{i}_c + \cancelto{0}{\mathbf{K}_s \mathbf{s}}$, the applied force can be expressed solely as a function of the AMB coil currents. This enables casting the equilibrium equations in matrix form as $\mathbf{A}\mathbf{x} = \mathbf{b}$ where $\mathbf{A}$ is a $4n \times 4$ matrix of measured control currents containing n discrete load steps spanning both increasing and decreasing external loads in all four loading directions. The current/force factors to be determined are contained in $\mathbf{x} = \left\{ K_{i,A_\zeta}, K_{i,A_\eta}, K_{i,B_\zeta}, K_{i,B_\eta} \right\}^T$, and $\mathbf{b}$ is a $4n \times 1$ vector containing the external forces applied using the calibration facility during the experimental procedure. The system of equations can be utilized to obtain the current/force factors by employing a Least Squares scheme.

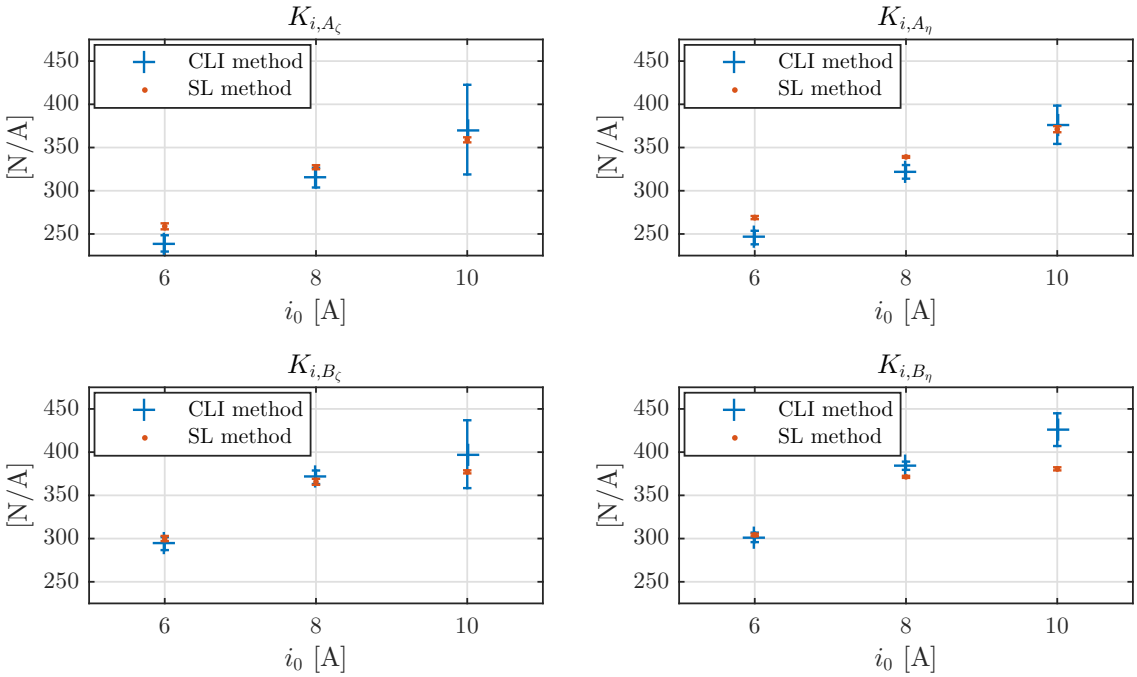

Fig. 4: K_i values for the different bias currents i_0. Top row, from left to right: $K_{i,A\zeta}$ for actuator ζ and $K_{i,A\eta}$ for actuator η in AMB A, respectively. Bottom row, from left to right: $K_{i,B\zeta}$ for actuator ζ and $K_{i,B\eta}$ for actuator η in AMB B, respectively. The error bars mark the 95 % confidence interval based on 5 repeated experiments.

6. Results

The main objective of this study is to determine the precision with which the parameters of a AMB-rotor can be estimated using the CLI methodology. To this end, the current/force factors, contained in $\mathbf{K}_i$, obtained experimentally using both the CLI and the SL approaches are used as a basis for a comparison of the two methods. Fig. 4 shows the $\mathbf{K}_i$ factors obtained for the three choices of bias currents. The plots includes errorbars indicating the 95 % confidence interval which is determined on the basis of five repeated tests conducted for both experimental methods. Good agreement between the results from the two methods are seen, with discrepancies below approximately 10 %. The $\mathbf{K}_i$ factors generally increase with the bias current and are similar for the two actuator directions ζ, η in each AMB, respectively. AMBs A and B are significantly different in terms of the magnitude of their respective current/force factors. The difference is mainly attributed to the different ways of manufacturing the AMB A and AMB B stators which ultimately leads to the nominal air gap of AMB A being 15 – 20 % smaller than the nominal air gap of AMB B. Furthermore, the current/force factors identified for AMB B using the SL method is seen to saturate when the bias current is increased above 8 A. This effect is not as pronounced for AMB A, and could be attributed to the fact that as the nominal air gap is smaller in AMB B compared to AMB A, leading to premature saturation of the AMB B stator. Additionally, saturation is an inherently non-linear phenomenon and consequently not captured by the assumed linear model structure upon which the CLI method is based. This is suspected to be of significant influence for the decrease in the overall fitting quality for the 10 A case included in Table 2. The fitting quality is determined as a Goodness of fit parameter using a normalized root mean square error approach.

In addition to current/force factors the CLI method is used to quantify the uncertain displacement/force factors. The results are summarised in Table 2. As expected the values of displacement/force factors are seen to increase for increasing bias currents and the two displacement/force factors values belonging to each AMB are approximately equal with higher values for AMB B again attributed to the geometrical differences between the AMB stators as discussed above. The Relative Standard Deviation (RSD) is calculated as the standard deviation in percent of the mean value of the displacement/force factors for all five tests and included in Table 2. The RSDs are generally low for the 6 A and 8 A cases, however larger for the 10 A case.

Table 2: Nominal K_s parameters identified with the CLI method. Additionally RSD values in percent calculated from the five repeated tests are included.

Bias current	6 A		8 A		10 A	
Actuator	k_s [N/m]	RSD [%]	k_s [N/m]	RSD [%]	k_s [N/m]	RSD [%]
A_ζ	$2.39 \cdot 10^6$	2.4	$4.09 \cdot 10^6$	1.9	$5.69 \cdot 10^6$	7.7
A_η	$2.49 \cdot 10^6$	2.1	$4.27 \cdot 10^6$	1.5	$5.94 \cdot 10^6$	3.0
B_ζ	$3.13 \cdot 10^6$	1.4	$5.16 \cdot 10^6$	1.1	$6.49 \cdot 10^6$	5.7
B_η	$3.19 \cdot 10^6$	1.1	$5.34 \cdot 10^6$	0.7	$7.00 \cdot 10^6$	2.3
Average fitting quality	95.2 %		93.4 %		84.5 %	

Table 3: Identified time constant τ_e for all bias current cases

Bias current	6 A		8 A		10 A	
Quantity	τ_e [s]	RSD [%]	τ_e [s]	RSD [%]	τ_e [s]	RSD [%]
Both AMBs	0.021	5.9	0.028	59	0.010	0.0

Finally the identified time constant τ_e is reported in Table 3. The values reported are the mean values and the RSD obtained from the five tests. For the 6 A and 8 A cases, τ_e is estimated within the same order of magnitude. For the 10 A case the CLI method returns a average value of τ_e which is significantly different than for the 6 A and 8 A cases. This is reflected in the very low average fitting quality values reported in Table 2 for the 10 A case, indicating that further variation of $\Delta\tau_e$ does not yield a better fit between simulated data and data obtained experimentally. This could indicate that the model fails to represent the electrodynamic behaviour of the AMB actuators for large bias currents due to the onset of non-linear operating regime under these conditions as discussed previously. The RSD values for the 6 A and 8 A are 5.9 % and 59 %, respectively and the growing RSD values could be a manifestation of the fact that the first order representation of the unknown actuator dynamics is insufficient, and the resulting τ_e should be used with care for high bias currents.

A representative visualisation of the performance of the CLI methodology is shown in Fig. 5, depicting both experimental and simulated time series responses for the imposed PRBS current perturbation. It is important to notice that the simulated results are obtained with the nine optimal parameters determined using Eq. (9). Good agreement between the experimental and simulated time series of lateral rotor displacements are seen in Fig. 5(a). The simulated versus measured AMB control currents for AMB B are seen in Fig. 5(b). Qualitatively good agreement is seen and the model captures the experimental trends, albeit significant noise levels are seen on the experimental data. High frequency oscillations are seen in the current signal obtained experimentally which the model fails to capture. This discrepancy could potentially be attributed to a too low model order for the commercial amplifiers. However, further research is required to establish if this is the case.

7. Conclusion and outlook

The CLI and SL methods produce similar results for $\mathbf{K}_i$, which indicates that the CLI method is able to perform closed loop identification of uncertain AMB parameters. The CLI method has proved very useful for providing quick, transparent and sufficiently accurate estimation of uncertain parameters during the controller tuning phase. The CLI method is orders of magnitudes faster than the SL method and does not require additional external hardware as the SL does. Additionally, the CLI method is general and allows for identification of multiple types of parameters such as $\mathbf{K}_i$, $\mathbf{K}_s$ and τ_e even for flexible rotor systems. However, the linear structure adopted in the presented formulation of the CLI method appears to lead to challenges in the non-linear operational domain of the AMBs. The non-linearities originate from saturation of the AMB actuators operated at high bias currents, for which the CLI methods over-predicts $\mathbf{K}_i$ compared to the the SL method. Furthermore, discrepancies between the simulated and measured current time series are suspected to originate from a too low model order for the amplifiers which is a relevant subject for future work. It is evident from the studies presented here that the electrodynamic model of the actuator requires additional attention. The embedded Hall sensor system of the AMBs could prove a powerful tool in this regard, as it enables quantification of the flux density generated in the stator. Consequently dynamics caused by the generation of Eddy currents in the AMB stators could potentially be quantified experimentally.

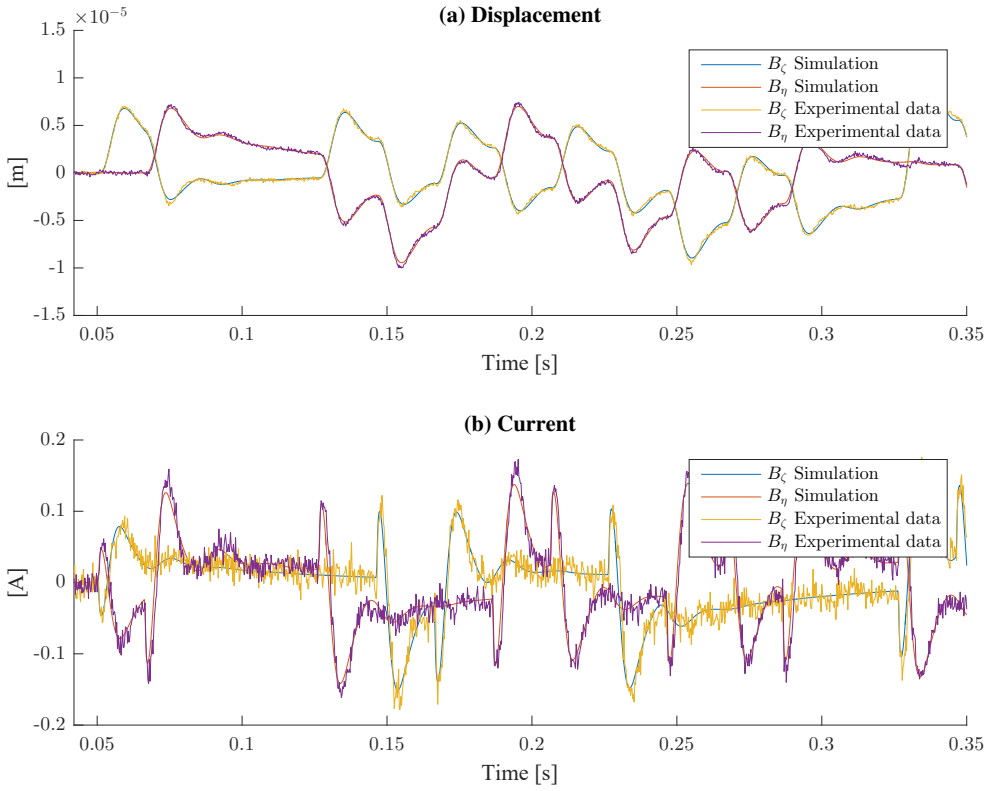

Fig. 5: Comparison of simulated and experimental data, here shown for AMB B. (a) Displacements and (b) control currents for a PRBS current input disturbance with an amplitude of 100 mA. Data obtained for a bias current of 6 A.

References

Schweitzer, G. "Active magnetic bearings - chances and limitations." IFToMM Sixth International Conference on Rotor Dynamics, Sydney, Australia. Vol. 1. 2002.

Anderson., B. D. From Youla Kucera to identification, adaptive and nonlinear control, Automatica 34, pp. 1485-1506, 1998.

Sun, Z., Zhao, J., Shi, Z. "Identification of magnetic bearing system using a novel subspace identification method" In Proceedings of ISMB14, pp. 87-90, 2014.

Sun, Z., He, Y., Zhao, J., Shi, Z., Zhao, L., Yu, S. "Identification of active magnetic bearing system with a flexible rotor." Mechanical Systems and Signal Processing 49.1 (2014): 302-316.

Tiwari, R., Chougale, A. "Identification of bearing dynamic parameters and unbalance states in a flexible rotor system fully levitated on active magnetic bearings." Mechatronics 24.3 (2014): 274-286.

Lauridsen, J. S., Sekunda, A. K., Santos, I. F., Niemann, H. "Identifying parameters in active magnetic bearing system using LFT formulation and Youla factorization." Control Applications (CCA), 2015 IEEE Conference on. IEEE, 2015.

Voigt, A. J., Mandrup-Poulsen, C., Nielsen, K. K., Santos, I. F. "Design and Calibration of a Full Scale Active Magnetic Bearing Based Testing Facility for Investigating Rotordynamic Properties of Turbomachinery Seals in Multiphase Flow". Proceedings of the ASME Turbo Expo 2016 (recommended for journal publication). Seoul, South Korea.

Bleuler, H., Cole, M., Keogh,P., Larsonneur, R., Maslen, E., Okada,Y., Schweitzer, G., Traxler, A. "Magnetic bearings: theory, design, and application to rotating machinery". Eds. Gerhard Schweitzer and Eric H. Maslen. Springer Science & Business Media, 2009.